

Efficiency and accuracy of numerical solutions to the time-dependent Schrödinger equationW. van Dijk,^{1,2} J. Brown,^{1,2} and K. Spyksma¹¹*Physics Department, Redeemer University College, Ancaster, Ontario, Canada L9K 1J4*²*Department of Physics and Astronomy, McMaster University, Hamilton, Ontario, Canada L8S 4M1*

(Received 19 July 2011; published 17 November 2011)

Recent significant improvements of the numerical solutions of the time-dependent Schrödinger equation beg the question as to whether these recent methods are comparable in efficacy (in terms of accuracy and computational time) to the current “method of choice,” i.e., the Chebyshev expansion of the time-evolution operator and the fast-Fourier-transform method of determining the kinetic energy. In this paper we review the methods in question and, by studying the time development of a coherent wave packet in an oscillator well, we are able to assess the effectiveness of the various methods. It turns out that the new generalizations come close (to within an order of magnitude) to being able to generate solutions as precisely and efficiently as the Chebyshev-fast-Fourier-transform method. The strict unitarity of the generalized methods may be an advantage. We also show that the fast-Fourier-transform approach to calculating the kinetic energy can be replaced by straightforward numerical differentiation to obtain the same precision.

DOI: [10.1103/PhysRevE.84.056703](https://doi.org/10.1103/PhysRevE.84.056703)

PACS number(s): 02.60.-x, 02.70.-c, 03.65.-w, 03.67.Lx

I. INTRODUCTION

The solutions of the time-dependent Schrödinger equation (TDSE) constitute the most fundamental description of nonrelativistic quantum processes evolving in time. Such processes are found in atomic and nuclear collisions, tunneling, laser-atom interactions, the dynamics of chemical reactions, decaying systems, quantum computational structures, and many other quantum phenomena. The paucity of analytic time-dependent solutions and the complexity of the interactions lead one to look for accurate numerical solutions.

Some recent, and ongoing, studies require improvements in the numerical methods in terms of accuracy, but also of efficiency, to make the calculations computationally feasible with current computer technology. This is the case with the study of α decay [1–3], and α decay with associated bremsstrahlung [1,4,5] or with coincident ionization [6]. The principal issue here is the lifetime of certain decaying nuclei, although extremely long half-life systems require significant approximations. Similar studies were done recently on proton emission during nuclear decay [7]. Even in model calculations [8,9] of quantum scattering leading to transitions between states the traditional methods fail to provide solutions with the precision or the efficiency to make the results meaningful or even possible.

Such solutions are also needed to study the basic unit of the “quantum abacus” [10]. The qubit here is an atom trapped in a harmonic well with a thin potential barrier at the center. The stability and robustness of the qubit and its proper functioning in quantum computing depend on the minimal degradation of a coherent wave packet over time. This quantum abacus is known to behave properly under ideal circumstances of a zero-width barrier. Numerical calculations for barriers with a realistic finite width, which may be complicated [11], are needed to determine the feasibility of such a device. Finally we mention the study of the time dependence of transmission of electrons in semiconductor superlattices [12,13]. In all these studies the original Crank-Nicolson method of solving the TDSE needs to be improved to obtain valid results. From these and like studies

it is evident that further advances in numerical approaches will enlarge the scope of systems that can be analyzed.

Since the early calculations using the Crank-Nicolson method [14], there have been improvements to obtain solutions more efficiently and with greater accuracy. A significant advance occurred in the 1980s when Tal-Ezer and Kosloff suggested a Chebyshev-polynomial expansion of the time-evolution operator [15]. Subsequently, Leforestier *et al.* [16] investigated a number of different propagation schemes and concluded that the Chebyshev propagation combined with the fast-Fourier-transform method of evaluating the action of the Hamiltonian on the wave function should be considered the “method of choice” for time-independent interactions. The advantage of this method is that it allows the calculation of the wave function at any later time without the necessity of making small steps in time in order to reach the final time. On the other hand, although the method can give very precise results, it is not unitary. The Crank-Nicolson method is explicitly unitary.

The recent generalizations of the Crank-Nicolson approach have lead to more precise solutions than the original. The work by Puzynin *et al.* [17,18] suggests the form of the generalizations. The time-evolution operator is expressed as a Padé approximant with the Hamiltonian multiplied by the time as argument. This method is still explicitly unitary; in fact, the choice of the diagonal Padé approximant makes it so. The method for obtaining the spatial dependence of the wave function is generalized by choosing a multi-point formula for the second-order spatial derivative [1] rather than the three-point formula. Another way of improving the determination of the spatial aspect of the wave function is that proposed by Muller [19] and Moyer [3] who introduce a Numerov-type three-point formula in the Crank-Nicolson approach. (See also Ref. [7].)

In 2007 van Dijk and Toyama [20], hereafter referred to as VT, fully generalized the Padé approximation for the time-evolution operator and used a $(2r + 1)$ -point formula for the second-order derivatives. In this way the precision of the calculation is improved by more than ten orders of magnitude

over the original Crank-Nicolson approach and the speed of calculation by more than four orders of magnitude. Two years later Shao and Wang [21], subsequently referred to as SW, further generalized the spatial aspect of the calculation by using a stencil for the second-order spatial derivatives that involved approximations to the second-order derivatives at a grid of points. This method is a generalization of the Numerov approach to the time-independent problem [3,19,21].

Because of the recent significant improvement over the traditional Crank-Nicolson method, it is timely to compare the efficiency and accuracy of the VT and SW methods with the Chebyshev expansion of the time-evolution operator method. In this paper we study and compare the three approaches of solving the time-dependent Schrödinger equation, i.e., the VT, SW, and the Chebyshev-propagation methods. With the latter method we consider an alternative to the fast-Fourier-transform (FFT) method of evaluating the Hamiltonian operation which is usually employed. The goal of this paper is to provide some practical guidelines for using these methods in cases where the exact solutions are not known, and to study the limitations of the various methods.

We are therefore concerned with finding the solution of the time-dependent Schrödinger equation

$$\left(i\hbar \frac{\partial}{\partial t} - H\right) \psi(x,t) = 0, \quad \psi(x,t_0) = \phi(x), \quad (1.1)$$

with the time-independent Hamiltonian

$$H = -\frac{\hbar^2}{2m} \frac{\partial^2}{\partial x^2} + V(x), \quad (1.2)$$

and with $\phi(x)$ as the wave function at initial time t_0 . The time-evolution operator $\exp(-iH\Delta t/\hbar)$ connects the wave function at time t to the one at a later time $t + \Delta t$, i.e.,

$$\psi(x,t + \Delta t) = e^{-iH\Delta t/\hbar} \psi(x,t). \quad (1.3)$$

Tal-Ezer and Kosloff [15] consider a Chebyshev expansion of this operator, whereas VT and SW use a Padé approximant approach. Furthermore the action of the Hamiltonian on the spatial aspect of the wave function is treated differently in all three papers.

We organize this paper as follows. In Sec. II we discuss the SW and the VT methods; the latter is formally a special case of the former. Section III describes the Chebyshev propagation method. In Sec. IV we compare the efficacy of the different methods in a model for which exact solutions exist. Finally Sec. V provides a discussion of the findings of the paper.

II. THE VAN DIJK-TOYAMA AND SHAO-WANG METHODS

The expansion of the time-evolution operator introduced by VT, and also employed by SW, is

$$e^{-iH\Delta t/\hbar} = \prod_{s=1}^M K_s^{(M)} + O((\Delta t)^{2M+1}), \quad (2.1)$$

where [22]

$$K_s^{(M)} = \frac{1 + (iH\Delta t/\hbar)/z_s^{(M)}}{1 - (iH\Delta t/\hbar)/\bar{z}_s^{(M)}}. \quad (2.2)$$

The quantities $z_s^{(M)}, s = 1, \dots, M$ are the (complex) roots of the numerator of the $[M/M]$ Padé approximant of the function e^z ; the $\bar{z}_s^{(M)}$ are the complex conjugates of the $z_s^{(M)}$, respectively. (In the following we will use the notation that the barred quantities are the complex conjugates of the corresponding unbarred quantities.)

Let us discretize the spatial coordinate x and the time t , i.e., $x_j = x_0 + j\Delta x, j = 0, 1, \dots, J$ and $t_n = t_0 + n\Delta t, n = 0, 1, 2, \dots$. We will assume that the wave function remains zero for $x \leq x_0$ and $x \geq x_J$ during the time of consideration. On the grid we obtain the numerical approximation of the wave function $\psi_{jn} \approx \psi(x_j, t_n)$. If we define the column vector $\Psi_n = (\psi_{0n}, \psi_{1n}, \dots, \psi_{jn}, \dots, \psi_{Jn})^T$, then

$$\Psi_{n+1} = e^{-iH\Delta t/\hbar} \Psi_n = \left(\prod_{s=1}^M K_s^{(M)} \right) \Psi_n. \quad (2.3)$$

This gives an approximation of the wave function after a time advance of Δt .

The Hamiltonian H of Eq. (1.2) involves a second-order derivative with respect to the spatial coordinate of the wave function. In their recent paper Shao and Wang [21] generalize the spatial-integration procedure to obtain the numerical wave function which is described in Ref. [20]. The idea is similar to the Numerov generalization for solving the second-order stationary-state differential equation. In that case the elementary three-point formula for the second-order derivative which is $O(h^4)$ is replaced by another which is $O(h^6)$ where h is the spatial step size. The latter formula is obtained by expanding the second-order derivative of the wave function as well as the wave function itself. (In order to simplify formulas we at times use h for Δx .)

To outline the derivation of both the VT and SW methods we consider that of SW and afterward indicate that the VT method can formally be regarded as a special case. SW consider the expansion of the second-order spatial derivative

$$y^{(2)}(x) = - \sum_{\substack{k=-r \\ (k \neq 0)}}^r a_k^{(r)} y^{(2)}(x + kh) - \frac{1}{h^2} \sum_{k=-r}^r c_k^{(r)} y(x + kh) + O(h^{4r}). \quad (2.4)$$

To obtain the coefficients $a_k^{(r)}$ and $c_k^{(r)}$ we make Taylor expansions of $y(x \pm kh)$ up to terms of $O(h^{4r})$; this results in

$$2 \frac{(kh)^2}{2!} y^{(2)}(x) + 2 \frac{(kh)^4}{4!} y^{(4)}(x) + \dots + 2 \frac{(kh)^{4r}}{(4r)!} y^{(4r)}(x) = y(x + kh) + y(x - kh) - 2y(x) + O(h^{4r+2}), \quad (2.5)$$

for $k = 1, \dots, r$. [See Eq. (2.7) of VT.]

Similarly we can make an expansion of $y^{(2)}(x \pm kh)$ and obtain for $k = 1, \dots, r$,

$$y^{(2)}(x) + \frac{(kh)^2}{2!} y^{(4)}(x) + \dots + \frac{(kh)^{4r-2}}{(4r-2)!} y^{(4r)}(x) = \frac{y^{(2)}(x + kh) + y^{(2)}(x - kh)}{2} + O(h^{4r}). \quad (2.6)$$

The system of equations formed by combining Eqs. (2.5) and (2.6) consists of $2r$ linear equations in $2r$ unknowns, i.e., $y^{(2)}(x), y^{(4)}(x), \dots, y^{(4r)}$. We can solve for $y^{(2)}(x)$ in terms of $y(x \pm kh), y(x), y^{(2)}(x \pm kh)$ for $k = 1, \dots, r$ and identify the coefficients $a_k^{(r)}$ and $c_k^{(r)}$ in Eq. (2.4). Since Eqs. (2.5) and (2.6) are symmetric under the interchange of k and $-k$, the coefficients also have that symmetry, i.e., $c_{-k} = c_k$ and $a_{-k} = a_k$.

In order to discuss the time evolution, let us first turn to the simple (first-order) Crank-Nicolson approximation to the time evolution, i.e., $M = s = 1$ and $z_1^{(1)} = -2$ in Eqs. (2.1) and (2.2). The generalization to more than one iteration for the higher-order approximation of the time-evolution operator is straightforward [20], and we will outline it subsequently. Thus

$$\left(1 + \frac{i\Delta t}{2\hbar} H\right) \psi(x, t + \Delta t) = \left(1 - \frac{i\Delta t}{2\hbar} H\right) \psi(x, t). \quad (2.7)$$

We now consider this expression as $x \rightarrow x + kh$, multiply by $a_{|k|}^{(r)}$, and sum over k from $-r$ to r . For $k = 0$ we

set $a_0^{(r)} = 1$.

$$\begin{aligned} \sum_{k=-r}^r a_{|k|}^{(r)} \left(1 + \frac{i\Delta t}{2\hbar} H\right) \psi(x + kh, t + \Delta t) \\ = \sum_{k=-r}^r a_{|k|}^{(r)} \left(1 - \frac{i\Delta t}{2\hbar} H\right) \psi(x + kh, t). \end{aligned} \quad (2.8)$$

Using Eq. (1.2) for H we write

$$\begin{aligned} \sum_{k=-r}^r a_{|k|}^{(r)} \left[1 - \frac{i\hbar\Delta t}{4m} \frac{\partial^2}{\partial x^2} + \frac{i\Delta t}{2\hbar} V(x + kh)\right] \psi(x + kh, t + \Delta t) \\ = \sum_{k=-r}^r a_{|k|}^{(r)} \left[1 + \frac{i\hbar\Delta t}{4m} \frac{\partial^2}{\partial x^2} - \frac{i\Delta t}{2\hbar} V(x + kh)\right] \psi(x + kh, t). \end{aligned} \quad (2.9)$$

Since according to Eq. (2.4)

$$\sum_{k=-r}^r a_{|k|}^{(r)} y^{(2)}(x + kh) = -\frac{1}{\hbar^2} \sum_{k=-r}^r c_{|k|}^{(r)} y(x + kh), \quad (2.10)$$

we obtain

$$\sum_{k=-r}^r \left\{ a_{|k|}^{(r)} \left[1 + \frac{i\Delta t}{2\hbar} V(x + kh)\right] + \frac{i\hbar\Delta t}{4mh^2} c_{|k|}^{(r)} \right\} \psi(x + kh, t + \Delta t) = \sum_{k=-r}^r \left\{ a_{|k|}^{(r)} \left[1 - \frac{i\Delta t}{2\hbar} V(x + kh)\right] - \frac{i\hbar\Delta t}{4mh^2} c_{|k|}^{(r)} \right\} \psi(x + kh, t). \quad (2.11)$$

To obtain the expression for a single iteration of the Padé approximant of the time-evolution operator, Eqs. (2.1) and (2.2), we replace $\Delta t/2$ with $-\Delta t/z_s^{(M)}$ on the left side of Eq. (2.11) and with $-\Delta t/\bar{z}_s^{(M)}$ on the right side, so that

$$\begin{aligned} \sum_{k=-r}^r \left\{ a_{|k|}^{(r)} \left[1 - \frac{i\Delta t}{\hbar z_s^{(M)}} V(x + kh)\right] - \frac{i\hbar\Delta t}{2mh^2 z_s^{(M)}} c_{|k|}^{(r)} \right\} \psi_{n+s/M}(x + kh) \\ = \sum_{k=-r}^r \left\{ a_{|k|}^{(r)} \left[1 + \frac{i\Delta t}{\hbar \bar{z}_s^{(M)}} V(x + kh)\right] + \frac{i\hbar\Delta t}{2mh^2 \bar{z}_s^{(M)}} c_{|k|}^{(r)} \right\} \psi_{n+(s-1)/M}(x + kh). \end{aligned}$$

This equation is an expression of the s th iteration of the one-step time-evolution operator; i.e., in notation that indicates the M intermediate steps from Ψ_n to Ψ_{n+1} ,

$$\Psi_{n+s/M} = K_s^{(M)} \Psi_{n+(s-1)/M}. \quad (2.12)$$

We can write

$$K_s^{(M)} = (A_s^{(M)})^{-1} \bar{A}_s^{(M)}, \quad (2.13)$$

where

$$(A_s^{(M)})_{j,j+k} = a_{|k|}^{(r)} \left[1 - \frac{i\Delta t V_{j+k}}{\hbar z_s^{(M)}}\right] - \frac{i\hbar\Delta t}{2mh^2 z_s^{(M)}} c_{|k|}^{(r)} \quad (2.14)$$

for $j = 0, 1, \dots, J$ and $k = -r, -r + 1, \dots, r$. The remaining elements $(A_s^{(M)})_{jj'}$ of the $(J + 1) \times (J + 1)$ matrix are zero.

We use the definition of $V_j \equiv V(x_j)$. Note that $A_s^{(M)}$ is a $(2r + 1)$ -banded diagonal matrix. Rather than using the iterative approach one could write

$$\left(\prod_{s=1}^M A_s^{(M)}\right) \Psi_{n+1} = \left(\prod_{s=1}^M \bar{A}_s^{(M)}\right) \Psi_n \quad (2.15)$$

and find the product matrices on both sides and use them to solve for Ψ_{n+1} from Ψ_n directly. Since the number of long operations (multiplication or division) for the banded diagonal matrix is $O(rJ)$, and the number of long operations in Gaussian elimination of a full matrix is $O(J^3)$, one expects that solving for intermediate wave functions is more efficient, especially for large J [23].

Let us cast this formulation into the form given by Shao and Wang. Divide Eq. (2.12) by $i\hbar\Delta t/(2mh^2)$ and take out the factor $1/z_s^{(M)}$ on the left side and $1/\bar{z}_s^{(M)}$ on the right. Let

$v_j = 2mV_j\hbar^2/\hbar$ and $\mu = 2m\hbar^2/\hbar$. Then

$$\begin{aligned} & \frac{1}{z_s^{(M)}} \sum_{k=-r}^r \left\{ a_{|k|}^{(r)} \left[\frac{\mu z_s^{(M)}}{i\Delta t} - v_{j+k} \right] - c_{|k|}^{(r)} \right\} \psi_{j+k, n+s/M} \\ &= \frac{1}{\bar{z}_s^{(M)}} \sum_{k=-r}^r \left\{ a_{|k|}^{(r)} \left[\frac{\mu \bar{z}_s^{(M)}}{i\Delta t} + v_{j+k} \right] + c_{|k|}^{(r)} \right\} \psi_{j+k, n+(s-1)/M} \end{aligned} \quad (2.16)$$

for $j = 0, 1, \dots, J$. These equations can be written as a matrix equation

$$\frac{1}{z_s^{(M)}} B_s^{(M)} \Psi_{n+s/M} = -\frac{1}{\bar{z}_s^{(M)}} \bar{B}_s^{(M)} \Psi_{n+(s-1)/M}, \quad (2.17)$$

where

$$(B_s^{(M)})_{j, j+k} = \begin{cases} c_{|k|}^{(r)} + a_{|k|}^{(r)} \left[v_{j+k} - \frac{\mu z_s^{(M)}}{i\Delta t} \right] & \text{for } |k| \leq r, \\ 0 & \text{otherwise.} \end{cases} \quad (2.18)$$

Writing the full equation in matrix form, we obtain

$$\begin{aligned} & \frac{1}{z_1^{(M)} z_2^{(M)} \dots z_M^{(M)}} \left(\prod_{s=1}^M B_s^{(M)} \right) \Psi_{n+1} \\ &= (-1)^M \frac{1}{\bar{z}_1^{(M)} \bar{z}_2^{(M)} \dots \bar{z}_M^{(M)}} \left(\prod_{s=1}^M \bar{B}_s^{(M)} \right) \Psi_n. \end{aligned} \quad (2.19)$$

Since the z 's are roots of a polynomial which are real or come in pairs of complex conjugates, the product of all of them is real and hence the prefactors, apart from the sign factor, cancel. Equation (2.16) can now be written as

$$\begin{aligned} & \sum_{k=-r}^r \left\{ c_{|k|}^{(r)} + a_{|k|}^{(r)} \left[v_{j+k} - \frac{\mu z_s^{(M)}}{i\Delta t} \right] \right\} \psi_{j+k, n+s/M} \\ &= -\sum_{k=-r}^r \left\{ c_{|k|}^{(r)} + a_{|k|}^{(r)} \left[v_{j+k} + \frac{\mu \bar{z}_s^{(M)}}{i\Delta t} \right] \right\} \psi_{j+k, n+(s-1)/M} \end{aligned} \quad (2.20)$$

for $j = 0, 1, \dots, J$. The last equation is equivalent to Eq. (2.19) of SW [24].

The approach of VT is formally a special case of the above derivation. One recovers those results by setting $a_k^{(r)} = -\delta_{k0}$ and evaluating the $c_k^{(r)} = b_k^{(r)}$ appropriately in Eq. (2.20). The system of linear equations that needs to be solved for the coefficients turns out to be different. Consequently the coefficients themselves will be unique for each method. To avoid confusion we will label the $c_k^{(r)}$ coefficients for the VT method as $b_k^{(r)}$.

III. CHEBYSHEV-POLYNOMIAL EXPANSION OF THE TIME-EVOLUTION OPERATOR

In an alternative approach the time-evolution operator is replaced by an expansion in terms of the orthogonal Chebyshev polynomials. Chebyshev polynomials of the first kind $T_n(x)$ are defined on the interval $[-1, 1]$. They satisfy the orthogonality

property using a scalar product involving a weight function $1/\sqrt{1-x^2}$,

$$\langle T_n(x), T_m(x) \rangle = \int_{-1}^1 \frac{T_n(x)T_m(x)}{\sqrt{1-x^2}} dx = C_n \delta_{nm}, \quad (3.1)$$

where $C_0 = \pi$ and $C_n = \pi/2$ for $n = 1, 2, 3, \dots$. Since the argument of the exponential in the time evolution operator [i.e., $\exp(-iH\Delta t/\hbar)$] is $-iH\Delta t/\hbar$, we use complex Chebyshev polynomials of the type $\phi_n(y) = i^n T_n(-iy)$ in the expansion. The orthogonality of the $\phi_n(y)$ is then expressed as

$$\langle \phi_n(y), \phi_m(y) \rangle = -i \int_{-i}^i \frac{\phi_n(y)\bar{\phi}_m(y)}{\sqrt{1-|y|^2}} dy = (-1)^n C_n \delta_{nm}, \quad (3.2)$$

where the weight function is now $-i/\sqrt{1-|y|^2}$ and the limits of integration are $-i$ and i . Like the Chebyshev polynomials of the first kind, the ϕ_n can be defined by the recursion relationship

$$\phi_n(y) = 2y\phi_{n-1}(y) + \phi_{n-2}(y), \quad (3.3)$$

where $\phi_0(y) = 1$ and $\phi_1(y) = y$.

The approach of Tal-Ezer and Kosloff [15] involves scaling the Hamiltonian so that its eigenvalues lie in the interval $[-1, 1]$. Suppose the eigenvalues of $H = \mathbf{p}^2/(2m) + V$ are $\lambda \in [E_{\max}, E_{\min}]$ where $E_{\min} = V_{\min}$, the minimum value of the potential energy, and $E_{\max} = \frac{\hbar^2 \pi^2}{2m(\Delta x)^2} + V_{\max}$ where V_{\max} is the maximum value of the potential energy. The scaled Hamiltonian is

$$H_{\text{scaled}} = \frac{H}{\Delta E} - \left(1 + \frac{E_{\min}}{\Delta E} \right), \quad (3.4)$$

where $\Delta E = (E_{\max} - E_{\min})/2$. Define $y \in [-i, i]$ as

$$y \equiv -i H_{\text{scaled}} = \frac{z}{\Delta E \Delta t / \hbar} + i \left(1 + \frac{E_{\min}}{\Delta E} \right) \quad (3.5)$$

with $z = -iH\Delta t/\hbar$.

Since z can be expressed in terms of y , we make the expansion

$$e^z = \sum_{n=0}^{\infty} a_n \phi_n(y), \quad (3.6)$$

where

$$\begin{aligned} a_n &= -i e^{-i(\Delta E + E_{\min})\Delta t/\hbar} \int_{-i}^i \frac{e^{\Delta E \Delta t y/\hbar} \bar{\phi}_n(y)}{\sqrt{1-|y|^2}} dy \\ &= e^{-i(\Delta E + E_{\min})\Delta t/\hbar} D_n J_n(\Delta E \Delta t/\hbar), \end{aligned} \quad (3.7)$$

where $D_0 = 1$, $D_n = 2$ for $n \geq 1$, and J_n is the Bessel function of the first kind. The time evolution of the system is described by the wave function so that

$$\psi(t + \Delta t) = e^{-iH\Delta t/\hbar} \psi(t) = e^z \psi(t), \quad (3.8)$$

where we have now taken the initial state to occur at time t . The wave function at the later time is

$$\psi(t + \Delta t) = e^z \psi(t) = \sum_{n=0}^{\infty} a_n \phi_n(y) \psi(t) = \sum_{n=0}^{\infty} a_n(\Delta t) \Phi_n(x), \quad (3.9)$$

where

$$\Phi_n \equiv \phi_n(y)\psi(t). \quad (3.10)$$

Then upon using the recursion relationship Eq. (3.3) we have

$$\begin{aligned} \Phi_0 &= \psi(t), \\ \Phi_1 &= y\psi(t) = y\Phi_0 = -\frac{i}{\Delta E} H\Phi_0 + i\left(1 + \frac{E_{\min}}{\Delta E}\right)\Phi_0, \\ \Phi_n &= -\frac{2i}{\Delta E} H\Phi_{n-1} + 2i\left(1 + \frac{E_{\min}}{\Delta E}\right)\Phi_{n-1} + \Phi_{n-2} \end{aligned} \quad (3.11)$$

for $n = 2, 3, \dots$. Note that Φ_n are members of the state-vector space, whereas the $\phi_n(y)$ are operators in that space.

This method can be used to obtain the wave function at some time from the initial wave function at an earlier time in one step. Alternatively one can obtain the final wave function by using a number of steps recursively. In that case the procedure is repeated for a particular value of Δt until a final time is reached. One needs to calculate the coefficients a_n only once and for each time step begin the iteration with the wave function calculated at the end of the previous time step. On the other hand it is perhaps numerically more economical to obtain the Φ_n once and for all, and calculate the coefficients a_n for each time in the grid in order to determine the wave function at each time.

A. Coordinate operator solution

The wave function ψ is a function of x and t . Up to now we have only indicated the time dependence. Since the Hamiltonian operator is

$$H = -\frac{\hbar^2}{2m} \frac{\partial^2}{\partial x^2} + V(x), \quad (3.12)$$

we consider an equally spaced grid of the domain of x of mesh size h and define the operator using the approach of Sec. II. Let $\chi(x)$ be a function which is operated on by H . The function at the grid points are denoted as χ_j . Thus

$$\begin{aligned} H\chi(x) &= -\frac{\hbar^2}{2m} \chi''(x) + V(x)\chi(x), \text{ or} \\ (H\chi)_j &= -\frac{\hbar^2}{2m} \chi''_j + V_j \chi_j. \end{aligned} \quad (3.13)$$

We form the sum

$$\sum_{k=-r}^r a_k^{(r)} (H\chi)_{j+k} = -\frac{\hbar^2}{2m} \sum_{k=-r}^r a_k^{(r)} \chi''_{j+k} + \sum_{k=-r}^r a_k^{(r)} V_{j+k} \chi_{j+k}. \quad (3.14)$$

Using Eq. (2.4) we can replace the first sum on the right side to obtain

$$\sum_{k=-r}^r a_k^{(r)} (H\chi)_{j+k} = \sum_{k=-r}^r \left(\frac{\hbar^2}{2mh^2} c_k^{(r)} + a_k^{(r)} V_{j+k} \right) \chi_{j+k}. \quad (3.15)$$

Thus if the χ_j are known we can obtain $(H\chi)_j$ by solving the system of equations. The coefficients $a_k^{(r)}$ on the right side form a banded diagonal matrix with the largest entry on the

diagonal multiplying the unknown vector $H\chi$, and therefore the system of equations can be solved by elementary means.

Alternatively we can use the approach of Ref. [20] in which the second-order spatial derivative is approximated as

$$y''(x) = \frac{1}{h^2} \sum_{k=-r}^r b_k^{(r)} y(x+kh) + O(h^{2r}). \quad (3.16)$$

The method of obtaining these coefficients is described in Ref. [20] Thus we can write Eq. (3.13) as

$$(H\chi)_j = \sum_{k=-r}^r \left(-\frac{\hbar^2}{2mh^2} b_k^{(r)} \chi_{j+k} \right) + V_j \chi_j. \quad (3.17)$$

This case does not necessitate solving a system of linear equations.

B. FFT method

One can use the fast-Fourier-transform (FFT) method to obtain the $\chi''(x)$ in $H\chi(x)$ of Eq. (3.13). The Fourier transform of $\chi(x)$ and its inverse transform are

$$\begin{aligned} X(\xi) &= \int_{-\infty}^{\infty} \chi(x) e^{2\pi i \xi x} dx, \\ \chi(x) &= \int_{-\infty}^{\infty} X(\xi) e^{-2\pi i \xi x} d\xi. \end{aligned} \quad (3.18)$$

By taking the second-order derivative with respect to x of the second equation, we obtain

$$\chi''(x) = -4\pi^2 \int_{-\infty}^{\infty} \xi^2 X(\xi) e^{-2\pi i \xi x} d\xi. \quad (3.19)$$

To obtain $\chi''(x)$ we first take the Fourier transform of $\chi(x)$, multiply it by $-4\pi^2 \xi^2$, and then do the inverse Fourier transform. Thus $H\chi(x)$ of Eq. (3.13) is obtained in a straightforward manner by combining $-(\hbar^2/(2m))\chi''(x)$ with the potential energy term. In this way one calculates the $H\Phi_{n-1}$ term in the recursive relationship for the Chebyshev-polynomial expansion of Eq. (3.11).

IV. COMPARISON OF THE DIFFERENT METHODS

In order to investigate the numerical efficiency of the various methods that have been described, we consider the exactly solvable coherent wave packet in an harmonic oscillator well. This example was also used by VT and SW and it was found that qualitatively it gave similar results as other examples, e.g., the propagating free wave packet.

In this case the potential energy and the initial wave function are

$$V(x) = \frac{1}{2} K x^2, \quad \psi(x, 0) = \frac{\alpha^{1/2}}{\pi^{1/4}} e^{-\alpha^2(x-a)^2/2}, \quad (4.1)$$

respectively, where $\alpha^4 = mK/\hbar^2$, $\omega = \sqrt{K/m}$, and a is the initial displacement of the packet. The exact wave function at later times is known. In the following we set $\hbar = m = 1$, $\omega = 0.2$, $a = 10$, $x_0 = -40$, $x_J = 40$, and $t_1 = 11T$, where the period $T = 10\pi$. The error e_2 is defined by the relation

$$(e_2)^2 = \int_{x_0}^{x_J} dx |\psi(x, t_1) - \psi_{\text{exact}}(x, t_1)|^2, \quad (4.2)$$

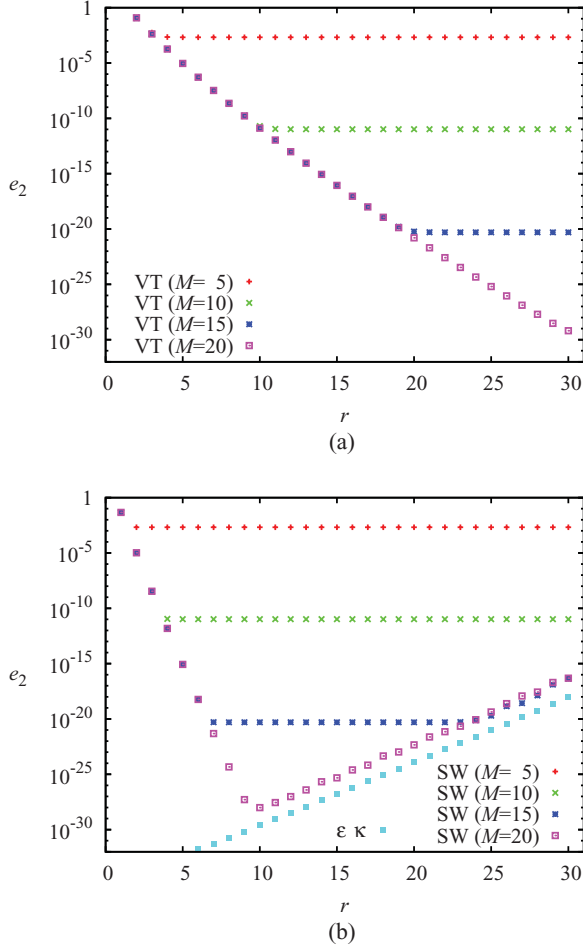


FIG. 1. (Color online) The error e_2 for a coherent wave packet in the harmonic oscillator well oscillating for eleven periods. In this calculation $\hbar = m = 1$, $\omega = 0.2$, $a = 10$, $\Delta t = T/40$, and $\Delta x = 0.2$. The error is plotted as a function of r for both the (a) VT and (b) SW methods. In (b), the lowest curve corresponds to the machine accuracy $\varepsilon = 10^{-34}$ times the condition number κ .

where $\psi_{\text{exact}}(x, t)$ is the analytic wave function for this solvable system.

A. Comparison of SW and VT numerics

We calculate e_2 as a function of r for various values of M . The graphs of the achievable precision of the SW and VT methods, Fig. 1, are quite instructive. Typically for the VT method as r increases for a given value of M the error e_2 decreases until a minimum value is reached after which it remains constant as r is increased further. The SW method gives a similar behavior except that for sufficiently large r the error e_2 increases with increasing r . The plateau values are dependent on M , but they are *identical for both* the VT and SW methods. The curves along which e_2 decreases is much steeper for SW than for VT. Overall the VT method is capable of greater precision since with increasing M and r the precision improves indefinitely. Thus if the demand for precision is not too great the SW method is preferred, but for extreme precision one might look to the VT method.

The graphs also indicate an independence of the precision obtained through the accuracy of the time evolution and through the accuracy of the spatial integration. The plateaux indicate that for certain values of M the precision is not dependent on r . The fact that outside the plateaux regions different values of M give identical errors for the same values of r also confirms this.

The behavior of the resulting errors can be explained in terms of the properties of the matrices involved in finding the solutions after a time step. Both methods call for the determination of the wave function from the matrix equation

$$A_s^{(M)} \Psi_{n+(s+1)/M} = \bar{A}_s^{(M)} \Psi_{n+s/M}, \quad (4.3)$$

where $A_s^{(M)} = (a_{jj'})_{N \times N}$ and the right side is known. This equation is solved for $\Psi_{n+(s+1)/M}$. (See VT for details.) For the VT method the matrix elements are

$$a_{jj'} = \begin{cases} 1 + \frac{i\hbar\Delta t}{2mh^2} \frac{b_0^{(r)}}{z_s^{(M)}} - \frac{i\Delta t/\hbar}{z_s^{(M)}} V_j, & j' = j, \\ \frac{i\hbar\Delta t}{2mh^2} \frac{b_{j-j'}^{(r)}}{z_s^{(M)}}, & 1 \leq |j - j'| \leq r, \\ 0, & \text{otherwise.} \end{cases} \quad (4.4)$$

Since the value of $|z_s^{(M)}|$ increases approximately linearly with M [20], the larger M the more likely that the matrix A is strictly diagonally dominant; i.e.,

$$\min \left\{ \left(|a_{jj}| - \sum_{j' \neq j} |a_{jj'}| \right), \text{ for all } j \right\} > 0. \quad (4.5)$$

In fact the diagonal dominance can be controlled by choosing $\hbar\Delta t/(2mh^2)$ appropriately. This property ensures that the matrix is well conditioned and Eq. (4.3) will have accurate solutions which are obtainable by simple Gaussian-elimination-type methods [25, page 48]. To be specific, a very conservative estimate derived in Appendix A that satisfies the condition (4.5) is

$$\frac{\hbar\Delta t}{2m(\Delta x)^2} < \frac{9M}{10(2r+1)}. \quad (4.6)$$

In fact the example of Fig. 1(a) shows that quantity on the right can be significantly larger.

We do a similar analysis for the SW method. Multiplying Eq. (2.20) through by $-i\Delta t/(\mu z_s^{(M)})$, we obtain matrix elements

$$a_{jj'} = \begin{cases} \left[1 - \frac{i\Delta t/\hbar}{z_s^{(M)}} V_j \right] a_{|j-j'|}^{(r)} - \frac{i\hbar\Delta t c_{|j-j'|}^{(r)}}{2mh^2 z_s^{(M)}}, & \text{for} \\ 0 \leq |j - j'| \leq r, & \\ 0, & \text{otherwise.} \end{cases} \quad (4.7)$$

The off-diagonal terms are as large in magnitude as the diagonal terms. One would expect that the stability of the solutions becomes compromised for larger r when the diagonal dominance is less likely. Thus we see that in Fig. 1(b) the solution for $M = 20$ deteriorates as r goes beyond ten.

Another way of seeing this is to consider the condition number $\kappa(A)$ of the matrix A [26, p. 319ff]. Since values of the condition number near unity indicate a well-conditioned matrix and large values an ill-conditioned one, we consider the quantity $\varepsilon\kappa$, where ε is the machine accuracy of the computation. If we calculate the average of the condition

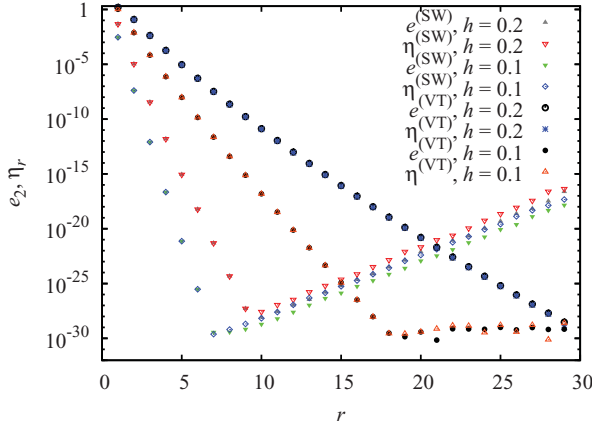


FIG. 2. (Color online) The error compared to the exact result e_2 and the difference of the last two approximations η_r . The parameters are those of Fig. 1 with $M = 20$ and $h = \Delta x$. In the legend on the figure the subscripts are omitted and the superscripts refer to the calculation used.

numbers of the M matrices $A_s^{(M)}$ of the SW method we obtain the lowest curve of Fig. 1(b), which is a graph of $\epsilon\kappa$ as a function of r . Remarkably this graph is very close to that of e_2 for $r \gtrsim 10$. The identical slopes indicate that the loss of precision is in step with the increase of the condition number as described in Ref. [27, pp. 94–98].

Usually there is no analytic solution by which the precision of the numerical solution can be tested. In that case we consider solutions of increasing precision and from those obtain an estimate of the error. Let us define the difference precision η_r of the last two approximations with successive values of r as

$$\eta_r = \int_{x_0}^{x_j} dx |\psi^{(r+1)}(x, t_1) - \psi^{(r)}(x, t_1)|^2, \quad \text{for } r = 1, 2, 3, \dots, \quad (4.8)$$

where $\psi^{(r)}(x, t)$ is the numerical wave function obtained with the $(2r + 1)$ -point formula for the second-order spatial derivative using some value of M for the time propagation. Hence in Fig. 2 we show the relationship between the differences in the last two obtained solutions and the error. Careful scrutiny of the graph shows that on the downward slopes of the curves $e_2 \approx \eta_r$ for both methods and both values of h . On the upward slopes of the curves belonging to the SW method η_r is slightly larger than e_2 , say by one order of magnitude. For the horizontal portion of the VT curve we have reached the limitation due to the machine precision of the computer and there is some random fluctuation of the values of e_2 and η_r around the horizontal plateau. Thus the values of e_2 and η_r track each other closely.

The CPU time [28] is slightly larger with the SW method than with the VT method for a given M and r as shown in Fig. 3. It should be noted however that the CPU times are given for the same r values but the spatial truncation error is $O(h^{4r})$ for SW and $O(h^{2r})$ for VT. Hence when the error due to ill-conditioned matrices has not set in yet, the SW method is much faster for a given precision.

When the example is the propagating free wave packet, the figures show similar results as for the coherent oscillating wave packet. Such figures are given in Appendix B.

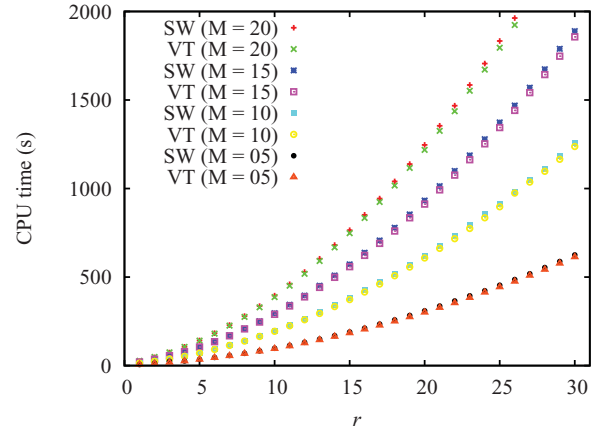


FIG. 3. (Color online) The CPU time for the coherent wave packet of Fig. 1.

B. Numerical comparisons of the Chebyshev-SW, -VT, and -FFT methods

In this subsection we compare the three versions of the Chebyshev-polynomial expansion of the time-evolution operator; for convenience we have labeled them CSW, CVT, and CFFT according to the method of evaluating the kinetic energy operator acting on the wave function. We again use the time evolution of a coherent wave packet as the test model. In Fig. 4 we plot e_2 as a function of r when the oscillator is allowed to evolve for eleven periods. Results for both the CVT and CSW methods are calculated. In order to make comparisons with the CFFT method we choose the number of intervals to be a power of 2. We observe behavior similar to that of the generalized Crank-Nicolson method (VT and SW). For instance the CSW reaches the greatest precision at lower values of r than the same precision obtained with CVT method. As before CSW reaches a greatest precision result for a particular value of r and then the precision deteriorates as r is increased further, whereas with the CVT method the greatest precision is reached at some value of r and then

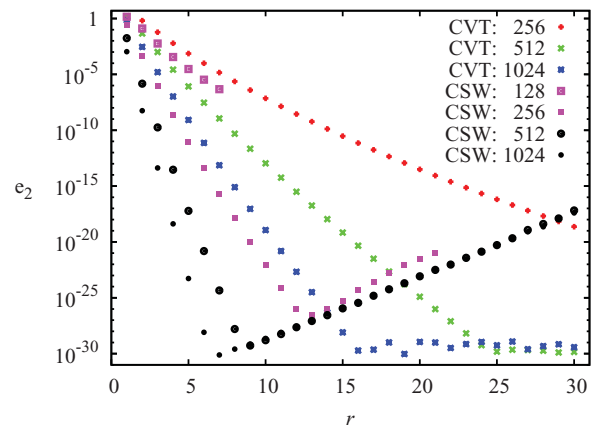


FIG. 4. (Color online) The error e_2 as a function of r of the coherent wave packet for the SW and VT approximation to H . The parameters of the potential and the length of time (eleven periods) are the same as in Sec. IV. The numbers in the legend refer to the number of subintervals in the partition of the spatial range.

TABLE I. CPU times for various calculations with the Chebyshev expansion of the time evolution operator. The model is the same as described in the caption of Fig. 1.

J	CFFT		CSW		CVT	
	CPU	e_2	CPU	e_2	CPU	e_2
128	30.6	2.22×10^{-11}	48.2	4.75×10^{-07}		
256	113	1.19×10^{-30}	417	2.72×10^{-27}	174	2.31×10^{-19}
512	652	1.28×10^{-30}	2813	5.35×10^{-30}	931	1.52×10^{-30}
1024	4818	1.53×10^{-30}	14608	7.59×10^{-31}	5938	9.27×10^{-31}

remains at that level as r is increased further. At this point $e_2 \approx 10^{-30}$ when calculations are performed with quadruple precision (approximately 34 significant digits). With the CSW this precision is reached only with the 1024 interval case, whereas with CVT this precision is achieved with all spatial partitions, although the smaller number of intervals may lead to inordinately large values of r .

It is surprising that such precision is obtained with Chebyshev method combined with the SW and VT expansions of the second-order spatial derivative. For instance, if in the 1024-subintervals case we consider the sum needed to evaluate the wave function

$$\psi(x, \Delta t) = e^{-i(\Delta E + E_{\min})\Delta t/\hbar} \sum_{n=0}^{n_{\max}} D_n J_n(\Delta E \Delta t/\hbar) \Phi_n(x), \quad (4.9)$$

we find that n_{\max} needs to be larger than 140 000 in order to reach the precision such that $e_2 \approx 10^{-30}$. Such a large number of terms is necessary in order to reach the order of the Bessel function so that the magnitude of subsequent Bessel functions falls off exponentially with order. In the recursion to obtain the $\Phi_n(x)$, in effect the second-order derivative of the function had to be taken this number of times. Normally one would not expect accurate results of numerical calculations of higher order derivatives; however, with the scaled Hamiltonian this is possible.

Note that in Fig. 4 the CSW calculations with 128 or 256 spatial intervals give results up to $r = 7$ and $r = 21$, respectively, after which the solutions become totally unreliable and e_2 escalates to unlimited values. Reducing the space of the solution so that, say, $-30 \leq x \leq 30$, allows for reliable solutions for larger values of r , but eventually the solutions still blow up. This is a result of values of $h = \Delta x$ being too large for the CSW method to be stable.

We compare CPU time of the various methods. Table I lists the CPU times with the error in the calculations as a function

TABLE II. CPU times for comparison of the VT method and the SW method. The model is the same as described in the caption of Fig. 1.

J	VT		SW	
	CPU	e_2	CPU	e_2
400	2478	6.51×10^{-30}	395	9.90×10^{-29}

of steps in the partition J . Table II gives the CPU times for the most precise (smallest e_2) calculations shown in Fig. 1.

From the numbers in Tables I and II it is apparent that the Chebyshev method with the fast-Fourier-transform (CFFT) method of determining the kinetic energy yields the most efficient calculations. In the CFFT calculations we have jumped to the final time in one step. This has an obvious advantage when one is interested in the final wave function. If however one wishes to have a set of wave functions on a time grid as is, for example, the case when studying the time propagation of a wave packet, then one has to do more calculation with the CFFT method whereas in the SW or VT method the wave functions are already calculated on a time grid. Thus the SW and VT methods are then of comparable efficiency to the method of choice, i.e., the CFFT method. The latter method is however not intrinsically unitary, although with the precision of the wave functions that were calculated this is not an issue.

V. DISCUSSION

Until recently the Chebyshev expansion of the time-evolution operator with the CFFT method of obtaining the kinetic energy yields the most efficient and precise numerical solution of the time-dependent Schrödinger equation. Given the right circumstances that may still be the case, but we have shown that the generalizations of the Crank-Nicolson method give numerical solutions of comparable precision and efficiency.

We can draw some further more particular conclusions from the work in this paper. We summarize them in point form. First we compare the SW and the VT methods.

(1) The SW method leads more efficiently to precise solutions than the VT method for relatively small values of r .

(2) For larger values of r the solutions of SW become less precise even though more computational effort is expended.

(3) The VT method's precision increases with r for all values of r and hence in principle is capable of greater precision.

(4) Since the VT method yields solutions whose precision increases monotonically with increasing M and r it is more straightforward to improve the calculations. However the SW method is more efficient for lower values of r and its precision can be estimated using the condition number. In both cases the difference $\eta_r - \eta_{r+1}$ can be used as an indicator of precision. If it is positive the precision has improved and either η_r or η_{r+1} gives an estimate of the error.

(5) Both methods are inherently unitary. The constraint due to unitarity is significant since it avoids exponential increases of unphysical components in the wave function introduced by

rounding errors [19]. It does not however prevent the wave function from becoming inaccurate when the step sizes are too large.

To summarize the comparisons of the Chebyshev FFT method and the generalized Crank-Nicolson methods, we list the following.

(1) The CFFT method is still somewhat superior, but the SW and VT methods are coming close in speed and accuracy.

(2) The Chebyshev expansion of the time-evolution operator accompanied by the numerical differentiation to obtain the kinetic energy is again slightly inferior to the CFFT method, but surprisingly it can be done with reasonable success.

(3) The Chebyshev expansion in principle fails to preserve unitarity, but for very precise solutions gives results which have preserved the normalization to a high degree.

Thus the generalized Crank-Nicolson methods do give us a viable alternative approach to obtain fast and accurate solutions to the time-dependent Schrödinger equation.

The generalized Crank-Nicolson methods are amenable to further generalization to solve cases with time-dependent potentials as indicated in Ref. [18]. Furthermore, there is revived interest in solutions of the nonlinear Schrödinger equation and the Gross-Pitaevski equation. The Chebyshev expansion for the time-dependent-potential case was recently done with proper care of the time-ordering in the time-evolution operator [29]. A similar approach using the Padé approximant of the time-evolution operator can be done by considering the time-dependent part of the Schrödinger equation as an inhomogeneous term [30,31]. The method of discretizing space has been extended to two dimensions for the time-independent Schrödinger equation [32]. This can readily be applied to the time-dependent Schrödinger equation. In the future we intend to investigate the two-dimensional case and the time-dependent-interaction case.

We have not considered the effect of boundary conditions at which the wave function and/or its spatial derivative is not zero. VT describe an approach for hard boundaries, which also applies to the origin of the radial wave equation. This approach has been tested for hard boundaries at both ends of the spatial region [33]. Further cases where the boundary is not impenetrable is discussed in Ref. [19]. In the case of the CFFT method such boundary conditions can be incorporated using endpoint corrections to the fast Fourier transforms. For third-order corrections in Δx see Ref. [34]. This approach can be generalized based on endpoint correction of regular integrals [35] or using the Euler-MacLaurin expansion with endpoint terms [36]. These corrections will make an insignificant difference in the precision and efficiency of the problem, provided they are applied to the same order as the main problem. As an aside, the Peters and Maley procedure [35] allows one to numerically evaluate the integrals involving the calculated wave function, e.g., the norm, very precisely using the simple rectangle-rule quadrature when the wave function is zero near the boundaries of the domain. In that case all endpoint corrections are zero and one achieves precision of $O(h^{2r})$ or $O(h^{4r})$.

It is evident that the grid size for the spatial and time variables are limited in order to give accurate solutions. Muller [19] pointed out that working in an appropriate gauge may significantly change the efficiency. Recently Bauke and

Keitel [37] explored in more detail the use of canonical transforms to be able to employ larger grid sizes leading to significant improvement of the numerical calculations. The gauge-transformed Hamiltonians are time dependent, and as mentioned above, to have a numeric procedure accurate to arbitrary order in Δt needs further investigation.

ACKNOWLEDGMENTS

This research is supported by the Natural Sciences and Engineering Research Council of Canada.

APPENDIX A: CONDITION FOR CONVERGENCE OF VT

Let us consider the condition for diagonal dominance (4.5) for the matrices of VT, Eq. (4.4). For simplicity assume that the potential is zero; i.e., $V_j = 0$. Then

$$a_{jj} = 1 + \frac{i\hbar\Delta t b_0^{(r)}}{2mh^2 z_s^{(M)}} = 1 + \frac{ivb_0^{(r)}(z_s^{(M)})^*}{|z_s^{(M)}|^2}, \quad (\text{A1})$$

where $v = \hbar\Delta t/(2mh^2)$. From this equation we obtain

$$|a_{jj}| = \sqrt{\left(1 + \frac{vb_0^{(r)}\text{Im}(z_s^{(M)})}{|z_s^{(M)}|^2}\right)^2 + \left(\frac{vb_0^{(r)}\text{Re}(z_s^{(M)})}{|z_s^{(M)}|^2}\right)^2} \geq \left|1 - \frac{v|b_0^{(r)}|}{|z_s^{(M)}|}\right|. \quad (\text{A2})$$

Using the fact that $|b_k^{(r)}| < |b_0^{(r)}|$ for $k \neq 0$, we obtain

$$|a_{jj'}| = \frac{v|b_{j-j'}^{(r)}|}{|z_s^{(M)}|}, \quad 1 \leq |j - j'| \leq r \leq \frac{v|b_0^{(r)}|}{|z_s^{(M)}|}. \quad (\text{A3})$$

Therefore

$$\sum_{j' \neq j} |a_{jj'}| \leq \frac{2rv|b_0^{(r)}|}{|z_s^{(M)}|}. \quad (\text{A4})$$

We observe that (see Ref. [20])

$$\frac{4}{3}M \leq |z_s^{(M)}| \leq \frac{9}{5}M \quad \text{and} \quad -3 \leq b_0^{(r)} \leq -2. \quad (\text{A5})$$

Along with these relations the diagonal dominance condition (4.5) can be used to obtain an estimate of the condition under which the solution is stable; i.e.,

$$v \equiv \frac{\hbar\Delta t}{2mh^2} \leq \frac{9M}{10(2r+1)}. \quad (\text{A6})$$

APPENDIX B: FREE PARTICLE PROPAGATION

We have repeated some of the analysis of Sec. IV for a free traveling wave packet as in Ref. [14]. The wave function of such a packet is the solution of the time-dependent Schrödinger

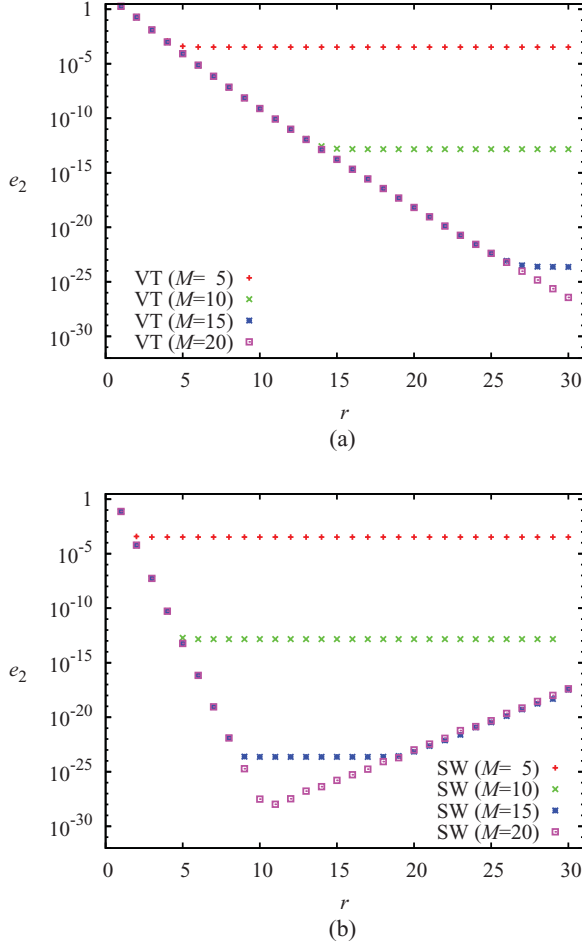


FIG. 5. (Color online) The error e_2 for the free wave packet. In this calculation $\hbar = 1$, $m = 1/2$, $k_0 = 50\pi$, $\sigma_0 = 0.05$, $x_0 = -0.75$, $x_N = 3.25$, $x_i = 0.25$, $\Delta x = 0.004$, $\Delta t = 0.0001$, and the final time $t_1 = 0.004$. The error at the final time is plotted as a function of r for both the VT (a) and the SW (b) methods when $M = 5, 10, 15, 20$.

equation with $V(x) = 0$ and can be written as

$$\psi(x,t) = (2\pi\sigma_0^2)^{-1/4} [1 + i\hbar t / (2m\sigma_0^2)]^{-1/2} \times \exp \left\{ \frac{-(x-x_i)^2 / (2\sigma_0)^2 + ik_0(x-x_i) - i\hbar k_0^2 t / (2m)}{1 + i\hbar t / (2m\sigma_0^2)} \right\}. \quad (\text{B1})$$

We use parameters similar to those of Ref. [14]. The units are chosen so that $\hbar = 1$ and $m = \frac{1}{2}$. The wave packet momentum is $\hbar k$. The initial wave function for the numerical

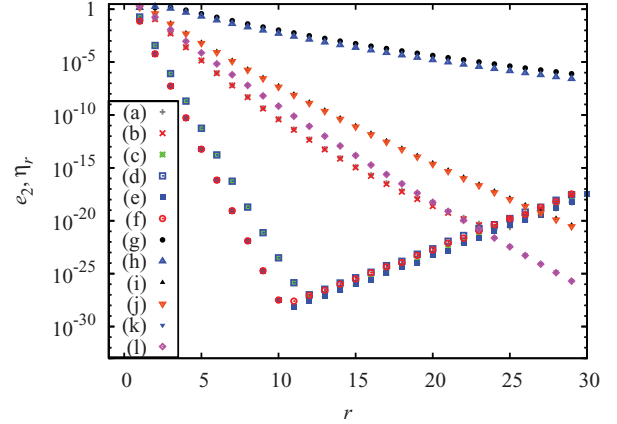


FIG. 6. (Color online) The error and precision of the final free wave packet. The legend is (a) e_2^{SW} with $h = 0.01$, (b) η_r^{SW} with $h = 0.01$, (c) e_2^{SW} with $h = 0.005$, (d) η_r^{SW} with $h = 0.005$, (e) e_2^{SW} with $h = 0.004$, (f) η_r^{SW} with $h = 0.004$, (g) e_2^{VT} with $h = 0.01$, (h) η_r^{VT} with $h = 0.01$, (i) e_2^{VT} with $h = 0.005$, (j) η_r^{VT} with $h = 0.005$, (k) e_2^{VT} with $h = 0.004$, and (l) η_r^{VT} with $h = 0.004$. All calculations were done with $M = 20$.

calculation is $\psi(x,0)$. The coordinate range we take from $x_0 = -0.75$ to $x_f = 3.25$ and the initial position of the wave packet is taken to be $x_i = 0.25$. We choose $\sigma_0 = 1/20$, $k_0 = 50\pi$, and the final time is $t_1 = 0.004$ with $\Delta t = t_1/40$. At the final position, which occurs at the final time, the numerically calculated wave function is compared to the analytic one and e_2 is determined, as well as η_r , when needed.

We present a graph similar to Fig. 1 but for the free wave packet in Fig. 5. Similarly we repeat the calculation that led to Fig. 2 for the free wave packet and show the results in Fig. 6. For Fig. 6 the chosen parameters for the spatial and temporal ranges are somewhat different. In that case we use $x_0 = -0.75$, $x_f = 3.75$, $x_i = 0.25$, and $t_1 = 0.004$ with $\Delta t = t_1/30$. Note that points for e_2 and η_r for identical parameters are virtually the same. The sets (g) and (h), and also (e) and (f), show the greatest differences although they are close. The sets (a) and (b) are interesting because they are the result of the SW calculation but seem to follow the pattern of VT calculations. A careful scrutiny shows however that the pattern bends at around $r = 23$ and merges with the upwardly sloped path typical of SW calculations.

Figures 5 and 6 show that the numerical behavior of the free wave packet when considered by the SW and VT methods is similar to that of the oscillating coherent wave packet and consequently the conclusions in Sec. V are more generally applicable than just to the oscillating coherent wave packet.

[1] Ş. Mişicu, M. Rizea, and W. Greiner, *J. Phys. G: Nucl. Part. Phys.* **27**, 993 (2001).
 [2] W. van Dijk, F. Kataoka, and Y. Nogami, *J. Phys. A: Math. Gen.* **32**, 6347 (1999).
 [3] C. A. Moyer, *Am. J. Phys.* **72**, 351 (2004).
 [4] C. A. Bertulani, D. T. de Paula, and V. G. Zelevinsky, *Phys. Rev. C* **60**, 031602(R) (1999).

[5] W. van Dijk and Y. Nogami, *Few-Body Syst. Suppl.* **14**, 229 (2003).
 [6] F. Kataoka, Y. Nogami, and W. van Dijk, *J. Phys. A: Math. Gen.* **33**, 5547 (2000).
 [7] M. Rizea, *J. Math. Chem.* **48**, 55 (2010).
 [8] W. van Dijk, K. A. Kiers, Y. Nogami, A. Platt, and K. Spyksma, *J. Phys. A: Math. Gen.* **36**, 5625 (2003).

- [9] W. van Dijk, K. Spykma, and M. West, *Phys. Rev. A* **78**, 022108 (2008).
- [10] T. Cheon, I. Tsutsui, and T. Fülöp, *Phys. Lett. A* **330**, 338 (2004).
- [11] T. Cheon and T. Shigehara, *Phys. Lett. A* **243**, 111 (1998).
- [12] C. N. Veenstra, W. van Dijk, D. W. L. Sprung, and J. Martorell, e-print arXiv:cond-mat/0411118v3.
- [13] D. W. L. Sprung, W. van Dijk, C. N. Veenstra, and J. Martorell, *Can. J. Phys.* **86**, 515 (2008).
- [14] A. Goldberg, H. M. Schey, and J. L. Swartz, *Am. J. Phys.* **35**, 177 (1967).
- [15] H. Tal-Ezer and R. Kosloff, *J. Chem. Phys.* **81**, 3967 (1984).
- [16] C. Leforestier, R. H. Bisseling, C. Cerjan, M. D. Feit, R. Friesner, A. Guldberg, A. Hammerich, G. Jolicard, W. Karrlein, H.-D. Meyer, N. Lipkin, O. Roncero, and R. Kosloff, *J. Comput. Phys.* **94**, 59 (1991).
- [17] I. Puzynin, A. Selin, and S. Vinitzky, *Comput. Phys. Commun.* **123**, 1 (1999).
- [18] I. Puzynin, A. Selin, and S. Vinitzky, *Comput. Phys. Commun.* **126**, 158 (2000).
- [19] H. G. Muller, *Laser Phys.* **9**, 138 (1999).
- [20] W. van Dijk and F. M. Toyama, *Phys. Rev. E* **75**, 036707 (2007).
- [21] H. Shao and Z. Wang, *Phys. Rev. E* **79**, 056705 (2009).
- [22] There is a misprint in Eq. (3.4) of Ref. [20]; the plus and minus signs should be interchanged.
- [23] To solve the problem using the product matrix means a product of M banded matrices. In each multiplication the band expands. With typical parameters of $J = 400$, $r = 20$, and $M = 20$ the band grows to a size so that the whole matrix is no longer diagonally banded.
- [24] The z 's of SW and ours are different by a factor of i , i.e., $z_v^{(L)}(\text{SW}) = iz_s^{(M)}(\text{VT})$, since we have expanded e^z as a rational function giving our z_s 's as roots of the numerator polynomial in z . SW on the other hand expand $e^{-i\epsilon}$ as a rational function of ϵ and their z_v 's are the zeroes of the numerator polynomial in ϵ .
- [25] W. H. Press, S. A. Teukolsky, W. T. Vetterling, and B. P. Flannery, *Numerical Recipes in C: The Art of Scientific Computing* (Cambridge University Press, Cambridge, 1988).
- [26] W. Cheney and D. Kincaid, *Numerical Mathematics and Computing*, 6th ed. (Thomson Brooks/Cole, 2008).
- [27] J. Wilkinson, *Rounding Errors in Algebraic Processes* (Prentice-Hall, 1963).
- [28] The CPU time is a measure relative to the computer used. The calculations of this paper were done on a computer with an AMD Opteron Processor 250 running at 2.4 GHz. The CPU times in seconds give a rough, but reproducible, comparison of the efficiency of the various methods.
- [29] M. Ndong, H. Tal-Ezer, R. Kosloff, and C. P. Koch, *J. Chem. Phys.* **132**, 064105 (2010).
- [30] M. Ndong, H. Tal-Ezer, R. Kosloff, and C. P. Koch, *J. Chem. Phys.* **130**, 124108 (2009).
- [31] W. van Dijk and F. M. Toyama (unpublished).
- [32] Z. Wang and H. Shao, *Comput. Phys. Commun.* **180**, 842 (2009).
- [33] W. van Dijk and M. West (unpublished).
- [34] W. H. Press and S. A. Teukolsky, *Comput. Phys.* **3**, 91 (1989).
- [35] G. O. Peters and C. E. Maley, *Am. Math. Mon.* **75**, 741 (1968).
- [36] D. W. L. Sprung, M. Betti, and W. van Dijk (unpublished).
- [37] H. Bauke and C. H. Keitel, *Phys. Rev. E* **80**, 016706 (2009).